Global feedforward control of spatio-temporal mechanical systems

Global Feedforward Control of Spatio-Temporal Mechanical Systems: With Application to a Prototype Wafer Stage

Robin de Rozario * **Robbert Voorhoeve** *
Wouter Aangenent ** **Tom Oomen** *

* *Eindhoven University of Technology, Department of Mechanical Engineering, P.O. Box 5600 MB Eindhoven (r.d.rozario@tue.nl)*
** *ASML Research Mechatronics and Control Technologies*

Abstract: High throughput requirements on high-precision manufacturing systems lead to a situation where the flexible dynamics hamper the performance at the positions of interest. Since these points are typically not measured directly, high performance local control of measured positions may lead to deteriorated performance due to internal deformations. A possible solution is to employ a control strategy which ensures that the desired rigid body motion is achieved, without exciting the parasitic flexible dynamics. In this paper, a feedforward controller design procedure is developed that achieves this type of global performance, which in turn leads to increased performance at the unmeasured positions of interest. The proposed method is applied to an experimental wafer stage showing that the proposed approach indeed leads to superior results with respect to the traditional local control approach.

Keywords: Motion control, Identification, Spatial, Feedforward, $\mathcal{H}_\infty$ control.

1. INTRODUCTION

Increasing accuracy and throughput requirements in high-precision mechatronic systems lead to a situation where the performance of unmeasured positions cannot be guaranteed by accurate control of measured positions (Oomen et al., 2015). In the traditional situation, these systems can be accurately approximated as a rigid body, which leads to a static relation between the measured and unmeasured positions. Feedforward control is exploited to achieve high tracking performance of the local positions, whereas feedback control is used to account for unmodelled disturbances (van de Wal et al., 2002). Increasing performance requirements and new designs lead to a situation where this traditional approach leads to undesirable behaviour due to internal flexible deformations (Boeren et al., 2015). Specifically since a dynamic relation now exists between the location where the sensor is measuring and the location where performance is desired. These dynamics need to be accurately modelled and explicitly taken into account by the controller in order to guarantee satisfactory performance. Moreover, the inferential dynamics become position-dependent in case the performance location changes during operation, as is shown in Figure 1 for a wafer stage. This results in a multivariable (MIMO), position-dependent, inferential control problem that needs to be adequately addressed to ensure the performance at unmeasured locations.

The inferential control problem received significant attention in the fields of process control (Brosilow and Joseph, 2002) and control of mechatronic systems (Oomen et al., 2015). This led to various control strategies including feedback and iterative learning control, Wallén et al. (2011), Hoelzle and Barton (2016), Bolder and Oomen (2016). In Oomen et al. (2015) a control-relevant identification and feedback controller design approach is presented that ensures the performance of the inferential variable. However, the presented technique is not directly applicable to position-dependent performance variables, nor is it tailored towards feedforward design. An alternative approach is present in Moheimani et al. (2003), where the identification and control of spatio-temporal systems is considered. By suitable formulation of a global induced norm, a Linear Time Invariant (LTI) controller can be synthesised that achieves optimal global performance.

Although important developments have been made to enhance the inferential performance of mechatronic systems through feedback, the optimal inferential feedforward problem for spatio-temporal systems has not yet been fully addressed. Therefore, the aim of this research is to develop a global optimal feedforward controller synthesis approach for these systems. This is achieved through the following contributions.

- C1 In Section 3, a class of spatio-temporal models is introduced and a framework is outlined for the identification of these systems.
- C2 In Section 4, a method is developed to synthesise global optimal feedforward controllers for spatio-temporal mechanical systems.
- C3 In Section 5, the proposed identification- and feedforward controller synthesis methods are applied to a prototype industrial wafer stage. The displayed superior inferential performance validates the proposed approach.

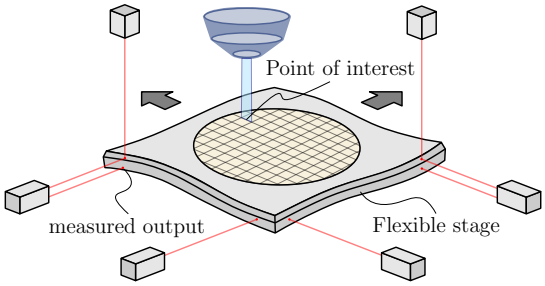

Fig. 1. A flexible stage that moves with respect to stationary sensors and illuminator results in a dynamic and position-dependent relation between the outputs and the point of interest.

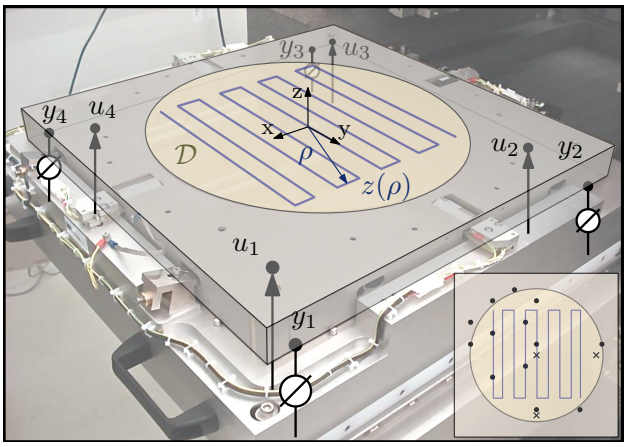

Fig. 2. Schematic layout of the setup. The inputs and outputs are indicated by u_i and y_i respectively. The performance variable $z(\rho)$ is the height of the stage at ρ, which varies over the wafer $\mathcal{D}$. The lower right corner shows the location of the additional actuators $\times$ and sensors $\bullet$ as used for system identification.

Contribution C1 is related to modal analysis and frequency domain system identification (Guillaume et al., 2003), in combination with multi-dimensional spline-based interpolation (Wahba and Wendelberger, 1980). In C2, novel controller design guidelines are presented that aim to optimize the inferential performance for systems which perform tracking motions, thereby extending the work in Moheimani et al. (2003). In the next section, the specific control problem is further elucidated.

2. PROBLEM FORMULATION

In this section, the control problem is formulated by means of the experimental case study. The latter serves as an illustrative example of the general methods developed here. To this end, the experimental case study is introduced first.

2.1 Experimental case study

The experimental setup, as is shown in Figure 2, serves as a case-study platform for the development of next-generation wafer stages. In this research, only the dynamics that result in a displacement in the z-direction are considered. The relevant inputs and outputs are indicated by u_i and y_i respectively and their locations on the wafer-stage are shown in Figure 2. On top of the stage, a wafer is located whose surface $\mathcal{D}$ needs to be illuminated. The point on the wafer that is to be illuminated is indicated by $\rho(t) \in \mathcal{D}$. To achieve the desired pattern, the surface

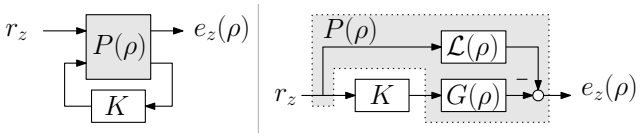

Fig. 3. Standard plant formulation of the position-dependent global feedforward control problem.

of the stage at ρ should levitate under the illuminator at a predefined height r_z. The actual height of the stage at ρ is indicated by $z(\rho)$, which is the position-dependent performance variable that should track the reference r_z. This problem can be tackled using a local or a global approach, as is discussed next.

2.2 Local and global inferential feedforward control

Inferential variables can be controlled using a global or local feedforward approach. To show the difference, let $G(\rho)$ be a system with position-independent input u and output y, and a position-dependent performance variable $z(\rho)$, then consider the following two problem statements.

Problem 1 (Local inferential feedforward)**.**
For a given local reference $r_z(t)$, find an input $u(t)$, such that the local tracking error $e_z(t) \triangleq r_z(t) - z(\rho(t))$ is small.

Problem 2 (Global spatial inferential feedforward)**.**
For a global reference $r_z(\rho, t)$, find an input $u(t)$, such that the tracking error $e_z(\rho, t) \triangleq r_z(\rho, t) - z(\rho, t)$ is small.

In Problem 1, the performance is considered locally at a certain point $\rho(t) \in \mathcal{D}$. By considering this performance location $\rho(t)$ as a scheduling variable, Linear Parameter-Varying techniques can be employed to solve this problem Rugh and Shamma (2000), Hoffmann and Werner (2015), de Rozario et al. (2017). In contrast, Problem 2 considers the spatial behaviour of the entire system. This is reflected by the spatial signal $z(\rho, t)$, which is a mapping from the time-axis to a function depending on ρ, which is a coordinate variable instead of a scheduling signal. In this paper, Problem 2 is considered, since it does not require the real-time availability of the performance location $\rho(t)$. This makes the global approach more robust, since all possible $\rho \in \mathcal{D}$ are considered simultaneously. Moreover, it will be shown in Section 4 that Problem 2 can be reformulated as an $\mathcal{H}_\infty$-optimal LTI feedforward problem, which can be efficiently solved using existing techniques. This reformulation is schematically shown in Figure 3, which requires that the involved signals are finite dimensional. This requirement is satisfied by approximating the true system by a finite finite-dimensional model $G(\rho)$ and by defining r_z as $r_z(\rho, t) \triangleq \mathcal{L}(\rho) r_\eta(t)$, with $\mathcal{L}(\rho)$ a row vector with spatial basis-functions and $r_\eta(t)$ is a column-vector with temporal coefficients. The identification of such finite-dimensional models $G(\rho)$ is key to solving either Problem 1 or 2 and will therefore be treated first in the next section.

3. IDENTIFICATION OF MECHANICAL SYSTEMS WITH SPATIO-TEMPORAL OUTPUTS

In this section, a framework is outlined for the identification of position-dependent systems, which is considered to be contribution C1. To this end, the relevant class of models is defined first by means of a first-principle approach in section 3.1. Then, a two-step identification

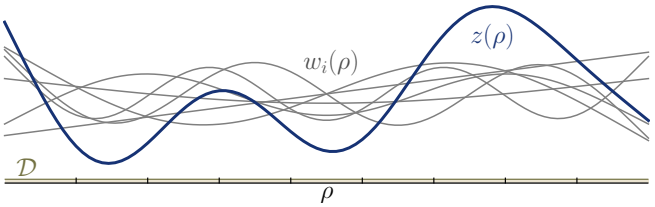

Fig. 4. Approximation of the surface $z(\rho)$ by basis functions $w_i(\rho)$ on the domain $\mathcal{D}$ in one dimension.

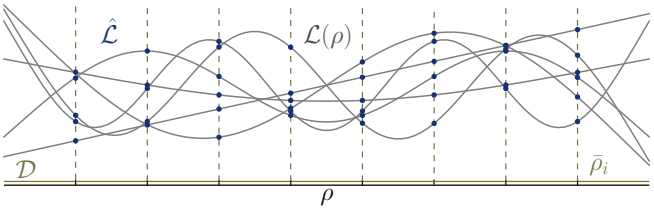

Fig. 5. The mode shapes are sampled on the fixed grid $\hat{\rho}$ by adding local outputs, such that they can be interpolated once these samples are estimated.

procedure is introduced in section 3.2. This procedure is applied to the experimental setup in section 5.1, which results in a position-dependent model of the experimental setup, that will be used in a model-based feedforward design procedure in section 5.2.

3.1 Model structure from first-principle modelling

In general identification methods for position-dependent or LPV systems, structure selection and model quality assessment are difficult when the model parameters have no physical interpretation. To overcome this, a first principle analysis is performed in this section, which reveals the grey-box structure of the relevant parametric model. The benefit of this approach is that the parameters have a physical interpretation, which significantly aids in estimating accurate spatio-temporal models. The quantity of interest is the surface of an unconstrained flexible single body $z(\rho, t)$. For the reasons of controller design and numerical tractability, it is desired to have finite dimensional description of $z(\rho, t)$. The latter is therefore approximated by a finite number of basis functions $w_i(\rho)$, as is shown in Figure 4 in one dimension, and is generally given by,

$$z(\rho, t) = W(\rho)q(t), \quad W(\rho) = [w_1(\rho) \ \dots \ w_{n_m}(\rho)],$$

where $q^\top(t) = [q_1(t) \ \dots \ q_{n_m}(t)]$ is the vector of temporal coefficients. Under the assumptions of linear strains and small rotations, and linear elastic material properties, the following equations of motion are obtained by applying Galerkin-projection to the partial differential equations of mass, momentum, and moment of momentum balance Eringer (1975),

$$\mathcal{M}\ddot{q}(t) + \mathcal{K}q(t) = Qu(t). \tag{1}$$

Here $\mathcal{M} = \mathcal{M}^\top \succ 0$ is the mass matrix, $\mathcal{K} = \mathcal{K}^\top \succeq 0$ the stiffness matrix and Q the input distribution matrix. The symmetry of the first two matrices is induced by the Galerkin projection and this allows a decoupling by solving the generalized eigenvalue problem $[\mathcal{K} - \omega_i^2\mathcal{M}]\phi_i = 0$, where ω_i are the natural eigenfrequencies of the system and ϕ_i are the corresponding undamped eigenmodes. Using mass-normalization and defining the natural coordinates as $\eta = \Phi^{-1}q(t)$, equation (1) can be written in modal form after pre-multiplication by $\Phi^\top$,

$$G(\rho): \begin{cases} I\ddot{\eta}(t) + D_m\dot{\eta}(t) + \Omega^2\eta(t) = \mathcal{R}u(t) & (2) \\ z(\rho, t) = \mathcal{L}(\rho)\eta(t), & (3) \end{cases}$$

where $\Omega^2 \triangleq \Phi^\top\mathcal{K}\Phi = \mathrm{diag}(\omega_i^2) \in \mathbb{R}^{n_m \times n_m}$, $\mathcal{R} \triangleq \Phi^\top Q \in \mathbb{R}^{n_m \times n_u}$ and $\mathcal{L}(\rho) \triangleq W(\rho)\Phi$. The term $D_m\dot{q}(t)$ is added to model the damping of the system, where $D_m \in \mathbb{R}^{n_m \times n_m}$ is full for general viscous damping and diagonal in the case of modal damping. Equations (2) and (3) represent the grey-box model that is to be estimated, where the unknown parameters are given by the matrices Ω^2, $\mathcal{R}$ and D_m and the vector of functions $\mathcal{L}(\rho)$. A two-step procedure to estimate these parameters from measured data is presented next.

3.2 A two-step identification procedure

First, the estimation of the continuous matrix function $\mathcal{L}(\rho)$ is considered. To this end, it can readily be seen from (3) that the entries of $\mathcal{L}(\rho)$ can be sampled by evaluating the deflection $z(\rho, t)$ on a set of coordinates $\hat{\rho}_i \in \mathcal{D}$ as is shown in Figure 5. This corresponds to adding outputs that measure the surface at the locations $\hat{\rho}_i$. By stacking these frozen outputs in the vector $\hat{z}$ as,

$$\hat{z}(t) = \begin{bmatrix} z(\hat{\rho}_1, t) \\ \vdots \\ z(\hat{\rho}_{n_\rho}, t) \end{bmatrix} = \hat{\mathcal{L}}\eta(t), \quad \hat{\mathcal{L}} = \begin{bmatrix} \mathcal{L}(\hat{\rho}_1) \\ \vdots \\ \mathcal{L}(\hat{\rho}_{n_\rho}) \end{bmatrix}, \tag{4}$$

then, the i-th row of $\hat{\mathcal{L}}$ contains a sample of each mode at $\hat{\rho}_i$, whereas the j-th column of $\hat{\mathcal{L}}$ contains the samples of the j-th mode on the entire grid $\hat{\rho}$. Hence, once $\hat{\mathcal{L}}$ is known, the mode shapes can be estimated by interpolating these columns. Note that equations (2) and (4) constitute a modal mechanical LTI system $\hat{G}$ in the input-output variables $u(t)$, $\hat{z}(t)$ and the latent variables $\eta(t)$. Hence, the following procedure leads to an estimate of $G(\rho)$.

- I1 Add n_ρ sensors that measure the surface of the system on a suitably chosen grid $\hat{\rho}$. Then identify the modal mechanical LTI model given by (2) and (4) by estimating the parameters, $\hat{\mathcal{L}}, \Omega^2, D_m, \mathcal{R}$.
- I2 Complete the mode shapes on $\mathcal{D}$ by interpolating the columns of $\hat{\mathcal{L}}$ on the grid $\hat{\rho}$.

Step I1 can be performed using techniques from modal analysis (Guillaume et al., 2003) or other system identification approaches that can handle structured models, whereas I2 is a general regression problem. In this research, a dedicated frequency domain identification approach is developed to solve I1 that can handle large input-output dimensions, enforce rigid body modes a priori and allows the incorporation of various forms of damping. This is followed by a smoothed thin plate splines regression approach as presented in Wahba and Wendelberger (1980) or alternatively by multivariate regression using basis-functions that represent the eigenmodes of a plate. This approach is applied to estimate a model of the experimental setup in Section 5. The algorithmic details are beyond the scope of this paper and are to appear elsewhere. In the next section, a method is developed compute a globally optimal feedforward controller based on a model $G(\rho)$.

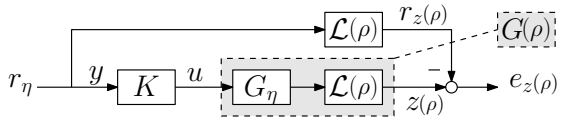

Fig. 6. Feedforward control scheme with K and G_η LTI systems and $\mathcal{L}(\rho)$ the basis of continuous modes that result in the spatial signals $z(\rho)$ and $r_z(\rho)$.

4. GLOBAL FEEDFORWARD CONTROL OF SPATIO-TEMPORAL MECHANICAL SYSTEMS

In this section, a method is proposed to synthesise feedforward controllers that achieve optimal global performance of position-dependent mechanical systems that perform tracking tasks. This constitutes contribution C2 and thereby solves Problem 2 as presented in Section 1. First in Section 4.1, the global optimal feedforward control problem is stated in detail by introducing spatial signals and their norms. Then in section 4.2, the equivalent $\mathcal{H}_\infty$ problem is derived and suitable design guidelines are provided. In section 5.2, the proposed approach is applied to the wafer stage.

4.1 Optimal global feedforward control

In this section, the global optimal feedforward control problem is posed. A discrete-time approach is taken here since the systems under consideration are assumed to be digitally controlled using a sample-and-hold implementation. This approach can be directly applied to the continuous time models that are identified in the section 3 in case a zero-order-hold implementation is used, since this leaves the output equation unaltered (Chen and Francis, 2012).

In the global approach as presented in problem 2, $r_z(\rho)$ and $z(\rho)$ are spatial signals, where a spatial discrete time signal s of dimension n_s is defined as a mapping $s : \mathbb{Z} \times \mathcal{D} \mapsto \mathbb{R}^{n_s}$. Recall that $z(k,\rho)$, given by (3) is represented by a finite sum of basis functions. To allow the same finite dimensional description of the tracking error $e(\rho)$, it is assumed that $r_z(\rho)$ can be equivalently described as, $r_z(\rho,k) = \mathcal{L}(\rho) r_\eta(k)$, with r_η a modal reference signal. This signal is fed to the feedforward controller, which leads to the scheme as shown in Figure 6, where G_η is given by equation (2) with output $\eta(k)$. The feedforward control problem can now be described as the effort of finding K such that the transfer $T(\rho) = \mathcal{L}(\rho)(I - G_\eta K)$ is small. To quantify the magnitude of the transfer $T(\rho)$, the weighted spatial l_2-norm of a spatial signal is defined as,

$$\|s\|_{2(\mathcal{D}_\Lambda)} \triangleq \sqrt{\sum_{k=-\infty}^{\infty} \int_{\mathcal{D}} s^\top(\rho,k)\Lambda(\rho)s(\rho,k)d\rho},$$

with $\Lambda(\rho) = \lambda(\rho)I$, where $\lambda(\rho)$ is a positive definite spatial weighting function on $\mathcal{D}$. Then, the control problem can be formulated in terms of minimizing the induced-norm $\|T(\rho)\|_{2(\mathcal{D}_\Lambda),2}$, as follows,

$$K = \arg \min_{K \in \mathcal{RH}_\infty} \sup_{\|r_z\|_2 = 1} \|e(\rho)\|_{2(\mathcal{D}_\Lambda)}. \tag{5}$$

This problem can be reduced to an $\mathcal{H}_\infty$-problem as is shown next.

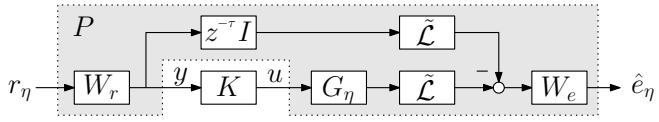

Fig. 7. The equivalent feedforward control scheme in standard plant formulation, augmented with input-output weights W_r and W_e, and a τ samples delay block which results in a controller K with preview.

4.2 The equivalent $\mathcal{H}_\infty$-problem

Problem 5 can be reduced to an $\mathcal{H}_\infty$-problem by computing an equivalent system $\hat{T}$ by extension of the approach in Moheimani et al. (2003), as follows.

Lemma 1. *Let $T(\rho) = \mathcal{L}(\rho)(I - G_\eta K)$, then it holds that,*

$$\|T(\rho)\|_{2(\mathcal{D}_\Lambda),2} = \|\tilde{T}\|_\infty,$$

with $\tilde{T} = \tilde{\mathcal{L}}(I - G_\eta K)$, where for $\tilde{\mathcal{L}} \in \mathbb{R}^{n_m \times n_m}$ holds that,

$$\tilde{\mathcal{L}}^\top \tilde{\mathcal{L}} = \Upsilon = \int_{\mathcal{D}} \mathcal{L}^\top(\rho)\Lambda(\rho)\mathcal{L}(\rho)d\rho. \tag{6}$$

The proof is provided in Appendix A, where it is also shown that $\Upsilon \succ 0$ and hence a Cholesky decomposition of Υ can be used to obtain $\tilde{\mathcal{L}}$ in lower-triangular form. Applying Lemma 1 to (5) and augmenting the problem with input-and-output weights W_r and W_e respectively, the following $\mathcal{H}_\infty$ control problem is obtained,

$$K = \arg \min_{K \in \mathcal{RH}_\infty} \|T_w\|_\infty,\ T_w = W_e \tilde{T} W_r. \tag{7}$$

At first sight, it seems that $I - G_\eta K = 0$ is the optimal solution. However, this can generally not be achieved since G_η non-square if more modes are modelled than there are actuators, i.e. $n_m > n_u$. Consequently, this problem can be viewed as obtaining a pseudo inverse K of G_η, such that the weighted residue T_w is minimal in the $\mathcal{H}_\infty$-norm. The weights can be used to specify the importance of the elements of $\tilde{T}$. For example, if it is assumed that the system $G(\rho)$ should perform rigid body tracking motions, while the flexible modes should be regulated, then the modal reference signal has the following structure, $r_\eta^\top = \begin{bmatrix} r_0^\top & 0^\top \end{bmatrix}$, with $r_0(k) \in \mathbb{R}^{n_0}$, with n_0 the number of rigid body modes. Hence, only the first n_0 columns of $\tilde{T}$ are of importance, which can be specified by taking for $i = 1, ..., n_0$,

$$W_r = \begin{bmatrix} W_{r_0} & 0 \\ 0 & 0 \end{bmatrix},\ W_{r_0} = \mathrm{diag}\{f_i\},\ f_i \in \mathcal{RH}_\infty. \tag{8}$$

Here W_r makes sure that the match between $G_\eta K$ and I is accurate in the first n_0 columns. Moreover, by taking f_i similar to the spectrum of r_0, emphasis is placed in the frequency region where suppression is crucial. Then by taking $W_e \in \mathbb{R}^{n_m \times n_m}$, the matrix $\tilde{\mathcal{L}}$ can be tuned manually. In this way, the resulting controller deviates from global optimality, but this allows the designer to tune the relative contribution of different modes to $z(\rho)$, which may benefit certain applications. Problem (7) can be solved using existing techniques as presented in Zhou et al. (1996), where the required standard plant formulation can be read from Figure 7, and is given by,

$$P : \begin{bmatrix} r_\eta \\ u \end{bmatrix} \mapsto \begin{bmatrix} \tilde{e} \\ y \end{bmatrix},\ P = \begin{bmatrix} W_e \tilde{\mathcal{L}} z^{-\tau} W_r & -W_e G_\eta \\ W_r & 0 \end{bmatrix}. \tag{9}$$

Note that additional τ samples of shift are introduced to obtain a finite preview feedforward controller as is

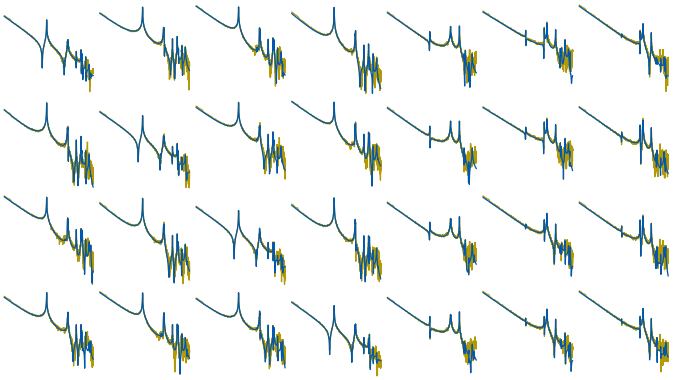

Fig. 8. A subset of the measured frequency response functions of the wafer stage and the parametric modal model that is identified in the frequency domain.

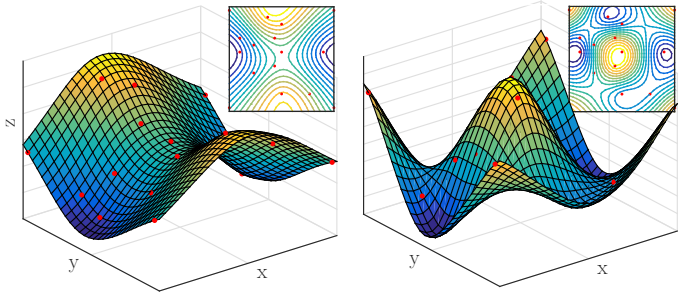

Fig. 9. Continuous completion of the 2nd and the 6th estimated flexible modes of the wafer stage.

discussed in Hazell and Limebeer (2008), which can lead to significantly increased performance. In the next section, the presented approach is applied to the wafer stage.

5. APPLICATION TO THE WAFER STAGE

In this section, the identification procedure as presented in Section 3 is used to estimate a model of the wafer stage as is shown in Figure 2. This model is then used to synthesise an optimal global controller as presented in section 4, whose superior performance is shown in a simulation example. This application of the presented methods constitutes contribution C3.

5.1 Spatio-temporal identification of the wafer stage

A spatio-temporal model $G(\rho)$ of the wafer stage is estimated by completing steps I1 and I2 as presented in Section 3. Following I1, additional surface sensors are put into place to enable the estimation of the continuous mode shapes. The augmented layout is shown in the lower right corner of Figure 2, which also shows a number of additional actuators which are used to optimally excite the modes. It is remarked that the locations of the sensors are selected based on mechanical constraints and such that the first 6 flexible modes are suitably sampled for subsequent interpolation. The LTI model $\hat{G}$ is estimated by fitting a modal model, as given by equations (2) and (4), to measured Frequency Response Function (FRF) data as is shown in Figure 8. The columns of $\hat{\mathcal{L}}$ of the resulting $\hat{G}$ are then interpolated using multivariate regression with two-dimensional Euler-Bernoulli basis functions. Figure 9 shows the result for the 2nd and the 6th flexible modes.

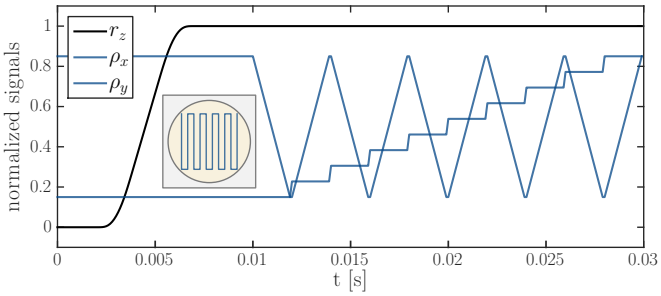

Fig. 10. Reference r_z, and the x, y-coordinates of the point of interest ρ over time.

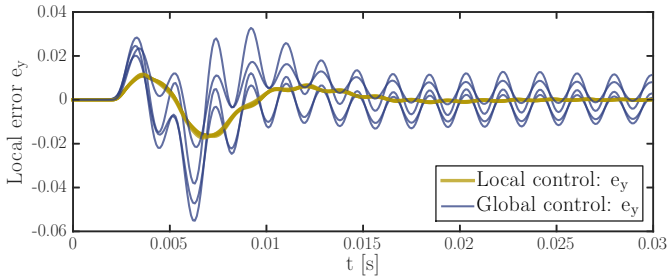

Fig. 11. Error at the local outputs y_i as shown in Figure 2, are smaller for the local controller, whereas the global controller allows a larger local error to improve the inferential performance as shown in Figure 12.

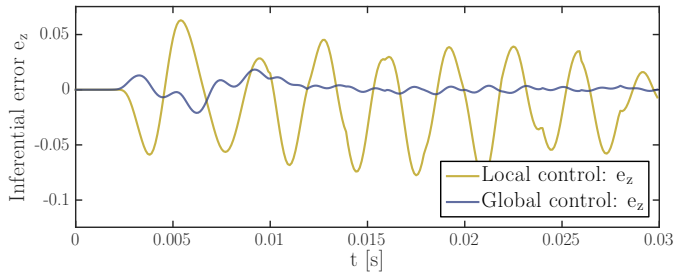

Fig. 12. The inferential error at the point of interest e_z of the global controller is much smaller than for the local controller, since the global controller explicitly takes the flexible dynamics into account.

5.2 Optimal global feedforward control of the wafer stage

The obtained model $G(\rho)$ is used to synthesise a global feedforward controller for the wafer stage. As presented in Section 1, the aim is to have the surface $z(\rho)$ follow r_z, at the point-of-interest ρ. Here, r_z is a fourth order point-to-point motion as is shown in Figure 10. This represents the tasks of bringing the stage into the focal plane of the illuminator, where it needs to stay without vibrating. The point-of-interest $\rho(t)$, moves across the surface in a back-and-fourth motion, as is shown there schematically. To achieve this, the global approach as presented in the previous section is applied to $G(\rho)$.

To this end, the continuous time model is discretised using zero-order-hold discretisation at a sample rate of 10 kHz. Note that this discretisation leaves $\mathcal{L}(\rho)$ unaltered so that (6) can be directly evaluated. No additional spatial weighting is used here, i.e., $\Lambda(\rho) = I$ and the integral is approximated using a two-dimensional trapezoidal scheme. The stage only has to perform a translation in the z-direction, and hence, only the first entry of r_η is taken to

be non-zero, since it corresponds to the translational rigid body mode. For W_r in (8) this leads to $W_{n_0} = f_1$, with f_1 a second order low-pass filter with a cut-off frequency of 1 kHz. Moreover, W_e is taken as, $W_{e,ii} = \alpha_i$, with $\alpha_i = 20$ for $i = 1, \ldots, 4$ and $\alpha_i = 1$ for $i > 4$. Due to the upper triangular form of $\tilde{\mathcal{L}}$, this choice of W_e emphasises the contribution of the first 4 modes. The $\mathcal{H}_\infty$-optimal controller K is obtained by solving (7) using the Matlab routine `hinfsyn.m`, where the standard plant P is given by (9). It is remarked here that at least $\tau \geq 2$ samples of preview are required to obtain a solution, due to the relative degree of $G(\rho)$. Moreover, the sampling zeros at the Nyquist frequency, as introduced by the discretisation, should be cancelled in order to avoid undesirable intersample behaviour and to improve the numerical conditioning of the optimisation problem.

The performance of the resulting global controller is compared to that of a classical $\mathcal{H}_\infty$-optimal controller that controls the local outputs y_i, whose locations $\bar{\rho}$ are shown in Figure 2. This controller is computed similarly, by formulating the standard plant as is shown in Figure 7, where $\tilde{\mathcal{L}}$ is replaced by $\bar{\mathcal{L}} = \mathcal{L}(\bar{\rho})$, $W_r = f_i I_4$ and $W_e = I_4$. For both controllers, $\tau = 5$ samples of preview are used, which results in the performance as shown in Figures 11 and 12. The first figure shows that at the local outputs y_i, the global controller allows a relatively large error, compared to the local controller, which is designed to achieve its performance there. By doing so, the global controller achieves superior inferential performance w.r.t. the local controller, as is shown in Figure 12. It is remarked here that in addition to the feedforward controller, a stabilising feedback is applied to the plant for both cases. The bandwidth of this controller is approximately 100 Hz which is such that its influence is negligible during the motion task, but it does counteract the rigid body drifting due to disturbances. This study shows that the traditional approach of controlling local outputs at the edges of a stage, does not guarantee performance at any other point. Hence, explicit modelling and controlling of the flexible dynamics is key to achieving the desired inferential performance.

6. CONCLUSION

In this paper, a two-step identification method is proposed to estimate spatio-temporal models of flexible mechanical systems. This is followed by the formulation a global feedforward design procedure to synthesise controllers that lead to superior inferential performance, as is shown by application to a wafer stage.

REFERENCES

Boeren, F., van Herpen, R., Oomen, T., van de Wal, M., and Steinbuch, M. (2015). Non-diagonal $\mathcal{H}_\infty$ weighting function design: Exploiting spatio-temporal deformations in precision motion control. *Control Engineering Practice*, 35, 35–42.

Bolder, J. and Oomen, T. (2016). Inferential iterative learning control: A 2D-system approach. *Automatica*, 71, 247–253.

Brosilow, C. and Joseph, B. (2002). *Techniques of model-based control*. Prentice Hall Professional.

Chen, T. and Francis, B.A. (2012). *Optimal sampled-data control systems*. Springer Science & Business Media.

de Rozario, R., Oomen, T., and Steinbuch, M. (2017). Iterative learning control and feedforward for LPV systems: Applied to a position-dependent motion system. In *Proc. Amer. Control Conf. (to appear)*. IEEE.

Eringer, A. (1975). *Elastodynamics*, volume 1. Academic Press.

Guillaume, P., Verboven, P., Vanlanduit, S., Van Der Auweraer, H., and Peeters, B. (2003). A poly-reference implementation of the least-squares complex frequency-domain estimator. In *Proc. of IMAC*, volume 21, 183–192.

Hazell, A. and Limebeer, D.J. (2008). An efficient algorithm for discrete-time $\mathcal{H}_\infty$ preview control. *Automatica*, 44(9), 2441–2448.

Hoelzle, D.J. and Barton, K.L. (2016). On spatial iterative learning control via 2-D convolution: Stability analysis and computational efficiency. *IEEE Trans. Control Sys. Technol.*, 24(4), 1504–1512.

Hoffmann, C. and Werner, H. (2015). A survey of linear parameter-varying control applications validated by experiments or high-fidelity simulations. *IEEE Trans. Control Sys. Technol.*, 23, 416–433.

Moheimani, S.R., Fleming, A.J., and Halim, D. (2003). *Spatial control of vibration: theory and experiments*, volume 10. World scientific.

Oomen, T., Grassens, E., and Hendriks, F. (2015). Inferential motion control: Identification and robust control framework for positioning an unmeasurable point of interest. *IEEE Trans. Control Sys. Technol.*, 23(4), 1602–1610.

Oomen, T., Van De Wijdeven, J., and Bosgra, O. (2009). Suppressing intersample behavior in iterative learning control. *Automatica*, 45(4), 981–988.

Rugh, W.J. and Shamma, J.S. (2000). Research on gain scheduling. *Automatica*, 36(10), 1401–1425.

van de Wal, M., van Baars, G., Sperling, F., and Bosgra, O. (2002). Multivariable $\mathcal{H}_\infty/\mu$ feedback control design for high-precision wafer stage motion. *Control Engineering Practice*, 10(7), 739–755.

Wahba, G. and Wendelberger, J. (1980). Some new mathematical methods for variational objective analysis using splines and cross validation. *Monthly weather review*, 108(8), 1122–1143.

Wallén, J., Norrlöf, M., and Gunnarsson, S. (2011). A framework for analysis of observer-based ILC. *Asian Journal of Control*, 13(1), 3–14.

Zhou, K., Doyle, J.C., Glover, K., et al. (1996). *Robust and optimal control*, volume 40. Prentice hall New Jersey.

Appendix A. PROOF OF LEMMA 1

Consider $\|e(\rho)\|_{2(\mathcal{D})} = \sqrt{\sum_{k=-\infty}^{\infty} \int_{\mathcal{D}} e^\top(\rho,k)\Lambda(\rho)e(\rho,k)d\rho}$ where from Figure 6 it is clear that $e(\rho) = \mathcal{L}(\rho)e_\eta$ with $e_\eta \triangleq (r_\eta - \eta)$. Hence, the spatial integral reads,

$$\int_{\mathcal{D}} e^\top(\rho)\Lambda(\rho)e(\rho)d\rho = e_\eta^\top \int_{\mathcal{D}} \mathcal{L}^\top(\rho)\Lambda(\rho)\mathcal{L}(\rho)d\rho e_\eta = e_\eta^\top \Upsilon e_\eta \geq 0,$$

with equality only if $e_\eta = 0$ if non of the entries of $\mathcal{L}(\rho)$ are identically zero. This implies $\Upsilon \succ 0$ and hence Υ can be factorized as $\Upsilon = \tilde{\mathcal{L}}^\top\tilde{\mathcal{L}}$ using the Cholesky decomposition. Consequently, $\sqrt{\sum_{k=-\infty}^{\infty} \int_{\mathcal{D}} e^\top(\rho,k)e(\rho,k)d\rho} = \sqrt{\sum_{k=-\infty}^{\infty} \tilde{e}_\eta^\top \tilde{e}_\eta} = \|\tilde{e}_\eta\|_2$, with $\tilde{e}_\eta = \tilde{\mathcal{L}}e_\eta$ and thus $\|e(\rho)\|_{2(\mathcal{D})} = \|\tilde{e}_\eta\|_2$. This in turn implies that $\|T(\rho)\|_{2(\mathcal{D}),2} = \|\tilde{T}\|_{2,2}$ which is equal to the $\mathcal{H}_\infty$ norm of $\tilde{T}$.